

The impact of the explicit representation of convection on the climate of a tidally locked planet in global stretched-mesh simulations.

DENIS E. SERGEEV ¹ IAN A. BOUTLE ^{2,1} F. HUGO LAMBERT ³ NATHAN J. MAYNE ¹ THOMAS BENDALL ²
KRISZTIAN KOHARY ¹ ENRICO OLIVIER ⁴ AND BEN SHIPWAY²

¹*Department of Physics and Astronomy, University of Exeter, Exeter, EX4 4QL, UK*

²*Met Office, Fitzroy Road, Exeter, EX1 3PB, UK*

³*Department of Mathematics and Statistics, University of Exeter, Exeter, EX4 4QF, UK*

⁴*Research Software Engineering, University of Exeter, Exeter, EX4 4QE, UK*

ABSTRACT

Convective processes are crucial in shaping exoplanetary atmospheres but are computationally expensive to simulate directly. A novel technique of simulating moist convection on tidally locked exoplanets is to use a global 3D model with a stretched mesh. This allows us to locally refine the model resolution to 4.7 km and resolve fine-scale convective processes without relying on parameterizations. We explore the impact of mesh stretching on the climate of a slowly rotating TRAPPIST-1e-like planet, assuming it is 1:1 tidally locked. In the stretched-mesh simulation with explicit convection, the climate is 5 K colder and 25% drier than that in the simulations with parameterized convection. This is due to the increased cloud reflectivity and exacerbated by the diminished greenhouse effect due to less water vapor. At the same time, our stretched-mesh simulations reproduce the key characteristics of the global climate of tidally locked rocky exoplanets, without any noticeable numerical artifacts. Our methodology opens an exciting and computationally feasible avenue for improving our understanding of 3D mixing in exoplanetary atmospheres. Our study also demonstrates the feasibility of a global stretched mesh configuration for LFRic-Atmosphere, the next-generation Met Office climate and weather model.

Keywords: Exoplanet atmospheres (487); Planetary atmospheres (1244); Habitable planets (695); Habitable zone (696); Atmospheric circulation (112)

1. INTRODUCTION

Fine-scale atmospheric phenomena such as moist convection, are typically unresolved in exoplanet climate models because the grid in these models is too coarse. Therefore, most general circulation models (GCMs) rely on convection parameterizations (Arakawa 2004). While convection parameterizations are physically motivated, they are necessarily a simplification of the real process (Kendon et al. 2021; Rios-Berrios et al. 2022). Recent studies showed that resolving convection explicitly may impact the estimate of the global climate of terrestrial tidally locked exoplanets (Sergeev et al. 2020; Lefèvre et al. 2021; Yang et al. 2023), because of the cloud stabilizing feedback (Yang et al. 2013). However, global convection-resolving simulations are computationally challenging, especially for climate-scale runs.

Locally refined global grids offer an elegant solution. They allow one to focus on a specific area of the planet, while keeping the global coverage and allowing for interactions at different scales, e.g. between localized convection and planetary-scale water distribution. Additionally, locally refined grids avoid numerical artifacts associated with using limited-area, or regional, models (Fox-Rabinovitz et al. 2008; Uchida et al. 2016). Namely, there are no boundaries or sharp changes in resolutions between the high-resolution region and the global model. These grids also allow for the two-way interaction between the region of interest and the rest of the planet, unlike a typical regional setup as in e.g.

Sergeev et al. (2020). This is especially important for the climate of tidally locked exoplanets, for which the localized stellar forcing is the key driving mechanism (e.g. Wordsworth & Kreidberg 2022).

A form of localized resolution increase is to stretch or deform the global mesh (e.g. Fox-Rabinovitz 2000; Uchida et al. 2016; Harris et al. 2016; Bindle et al. 2021). The advantages of this method are that the mesh remains topologically the same and does not require modifications to the model transport schemes. Grid stretching is also performed gradually, resulting in fewer grid artifacts compared to other methods. On the other hand, grid stretching typically results in a lower resolution on the opposite side of the planet, though it was not found to noticeably degrade the solution (Harris et al. 2016).

Stretched grids have been successfully applied for modeling Earth’s atmosphere, bringing improvements in reproducing phenomena such as tropical precipitation (Harris et al. 2016) and localized greenhouse gas emissions (Bindle et al. 2021). The topological simplicity of stretched grids has been shown to be particularly useful for simulating extreme precipitation and tropical cyclones in aquaplanet Earth simulations (Harris et al. 2016). Despite a substantial degree of stretching, there was no degradation of the global climate in these simulations and no spurious numerical noise contaminating the solution. An intercomparison of several stretched-mesh GCMs was shown to successfully reproduce the key aspects of regional climate (Fox-Rabinovitz et al. 2006), in which the major positive impact was due to a better representation of model dynamics and orography (Fox-Rabinovitz et al. 2008).

Tidally locked exoplanets offer an excellent use case for stretched-mesh GCMs because convective processes are hypothesized to occur mostly on the hot day side, on which the local refinement can be centered. Our work is the first application of a stretched-mesh GCM for the case of a tidally locked terrestrial exoplanet. We perform four experiments, in which we move from a configuration with a quasi-uniform mesh with parameterized convection to a stretched mesh with explicit convection. This includes an experiment with a “reduced” parameterization, serving as an intermediate step between fully parameterized and explicit convection. We demonstrate that it is computationally feasible to maintain the simulation fidelity of the global climate and at the same time resolve mesoscale circulations associated with the moist convection. Our stretched-mesh simulations resolve fine-scale cloud patterns on the day side to a similar degree as was done previously in limited-area (Zhang et al. 2017; Sergeev et al. 2020; Lefèvre et al. 2021) and pseudo-global (Yang et al. 2023) high-resolution simulations. Using an explicit convection configuration on a stretched mesh leads to a colder, lower relative humidity climate, and an increase in cloud water content and the rate of the most intense precipitation. At the same time, the structure of the large-scale atmospheric circulation typical for tidally locked terrestrial exoplanets is preserved, and mesh stretching does not produce any numerical artifacts.

2. METHODS

We use LFRic-Atmosphere, the new 3D GCM of the Met Office (Adams et al. 2019), based on a novel dynamical core GungHo and a suite of well-tested physical parameterizations inherited from its forerunner, the Unified Model (UM). GungHo solves the fully compressible non-hydrostatic Euler equations on a quasi-uniform cubed-sphere mesh using a mimetic finite-element discretisation and a mass-conserving finite-volume transport scheme (Melvin et al. 2019; Bendall et al. 2020, 2022; Kent et al. 2023). LFRic-Atmosphere reproduces a variety of atmospheric flows (Melvin et al. 2019; Kent et al. 2023; Brown et al. 2023; Melvin et al. 2024), including climate benchmarks for terrestrial exoplanets (Sergeev et al. 2023).

Our simulation parameters are based on the TRAPPIST-1 Habitable Atmosphere Intercomparison (THAI, Fauchez et al. 2020), a set of steady-state climate scenarios for a tidally locked TRAPPIST-1e assuming a 1 bar atmosphere. Sergeev et al. (2023) have shown that LFRic-Atmosphere reproduces the THAI scenarios close to that obtained from other models (e.g. Turbet et al. 2022; Wolf et al. 2022; Paradise et al. 2022). Here, we use the nitrogen-dominated aquaplanet case, *Hab 1* (Sergeev et al. 2022b), to highlight the impact of mesh stretching on cloud regimes and moist convection.

Importantly, we set the rotation period of the planet to be 12.2 days, i.e. twice as long as the one used in the THAI scenarios, while still assuming the planet is tidally locked. This is to avoid the climate bistability that often appears in 3D GCM simulations of the *Hab 1* case (Sergeev et al. 2022a) and would complicate our analysis, which is focused on the impact of the grid resolution. However, for any given case of a tidally-locked exoplanet within a similar region of parameter space, our findings are still pertinent. Additional simulations with the original rotation rate of 6.1 days indeed result in two distinct climate regimes, as we discuss in Appendix C.

Throughout this study we use the C192 cubed-sphere mesh, in a stretched and non-stretched configuration (see Appendix A for more details on mesh stretching). We performed four experiments: three with the mesh stretched by

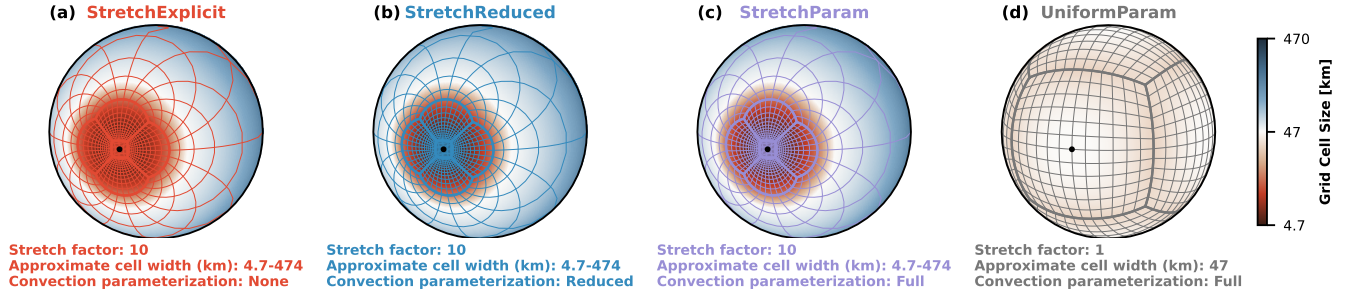


Figure 1. Summary of the simulation setup. Color shading shows the cell width (km) calculated as a square root of the cell area. All simulations use the C192 mesh. For clarity, the mesh edges are displayed at a low resolution (C12), so the actual grid cells in our simulations sixteen times smaller. The black dot shows the location of the substellar point. For more details on the stretching procedure, see Appendix A. Here and throughout the paper, the experiments are color-coded: *StretchExplicit* is shown in red, *StretchReduced* in blue, *StretchParam* in purple, and *UniformParam* in gray.

a factor of 10, and one with a non-stretched, quasi-uniform mesh (Fig 1), Appendix A). In the *UniformParam* and *StretchParam* configuration we use the same parameterizations as those used in Sergeev et al. (2023), including the standard mass-flux parameterization of convection. The *StretchParam* experiment differs from *UniformParam* only in the mesh configuration, while the *StretchReduced* experiment uses a reduced convective parameterization (Tomassini et al. 2023). The parameterization changes which are included in *StretchReduced* (for details, see Appendix B) are designed to allow small, unresolved convection to still be handled by the parameterization, whilst allowing larger and deeper convection to be explicitly resolved, and thus serves as an intermediate step between fully parameterized and fully explicit convection. The *StretchReduced* configuration, which can also be thought of as a “shallow-only” convection scheme, thus serves as an intermediate step between fully parameterized and explicit convection. The *StretchExplicit* configuration handles convection explicitly, i.e. with the parameterization switched off (see discussion in Sergeev et al. 2020).

All four experiments have 63 levels with a model top at about 41 km. This corresponds to the same vertical resolution below 41 km as that used by the Met Office’s Unified Model in global climate simulations (Walters et al. 2019; Tomassini et al. 2023). While the vertical resolution may impact the degree of convective aggregation (Jenney et al. 2023), the simulations for tidally locked terrestrial planets have not been sensitive to it (Wei et al. 2020; Yang et al. 2023). The impact of the vertical resolution in a stretched-mesh configuration will be investigated in a future study.

All simulations start from a dry isothermal (300 K) atmosphere at rest (Fauchez et al. 2020). We integrate the model for 1000 Earth days, which is sufficient, given the relatively thin atmosphere and the shallow (1 m) slab ocean at the bottom boundary (judging by the surface temperature and top-of-atmosphere energy balance reaching a steady state). Discarding the spin-up period, in Sec. 3 we present climate diagnostics for the final 500 days.

3. RESULTS

Adopting a refined mesh allows us to simulate convective clouds covering the substellar area in great detail. As the snapshots in Fig. 2a–d show, the stretched-mesh simulations produce spatial patterns of total column cloud condensate and precipitation rate similar to those reported in a convection-permitting limited-area model (Sergeev et al. 2020). The coarse, quasi-uniform mesh, on the other hand, produces a smoother pattern with a smaller variation of cloudiness and less extreme rainfall.

The stretched-mesh simulation without a convection parameterization (*StretchExplicit*), reproduces the so-called “cloud streets” on the day side’s periphery (Fig. 2a). These parallel elongated bands of clouds with cloud-free conditions between them were reported by Yang et al. (2023) in quasi-global convection-permitting simulations for TRAPPIST-1e. They form as a result of the persistent advection of cold air from the night side onto a warmer ocean surface of the day side, resulting in a formation of convective boundary layers. This is similar to the roll convection occurring in cold-air outbreaks on Earth (e.g. Gryschka & Raasch 2005). Our work supports the results from Yang et al. (2023) and demonstrates that cloud streets can be reproduced in a stretched-mesh global model at a reduced computational cost.

The small-scale variability enabled by the mesh refinement and explicit convection is also reflected in a marked increase in the precipitation rate in the substellar region. As Fig. 2h shows, the maximum instantaneous precipitation

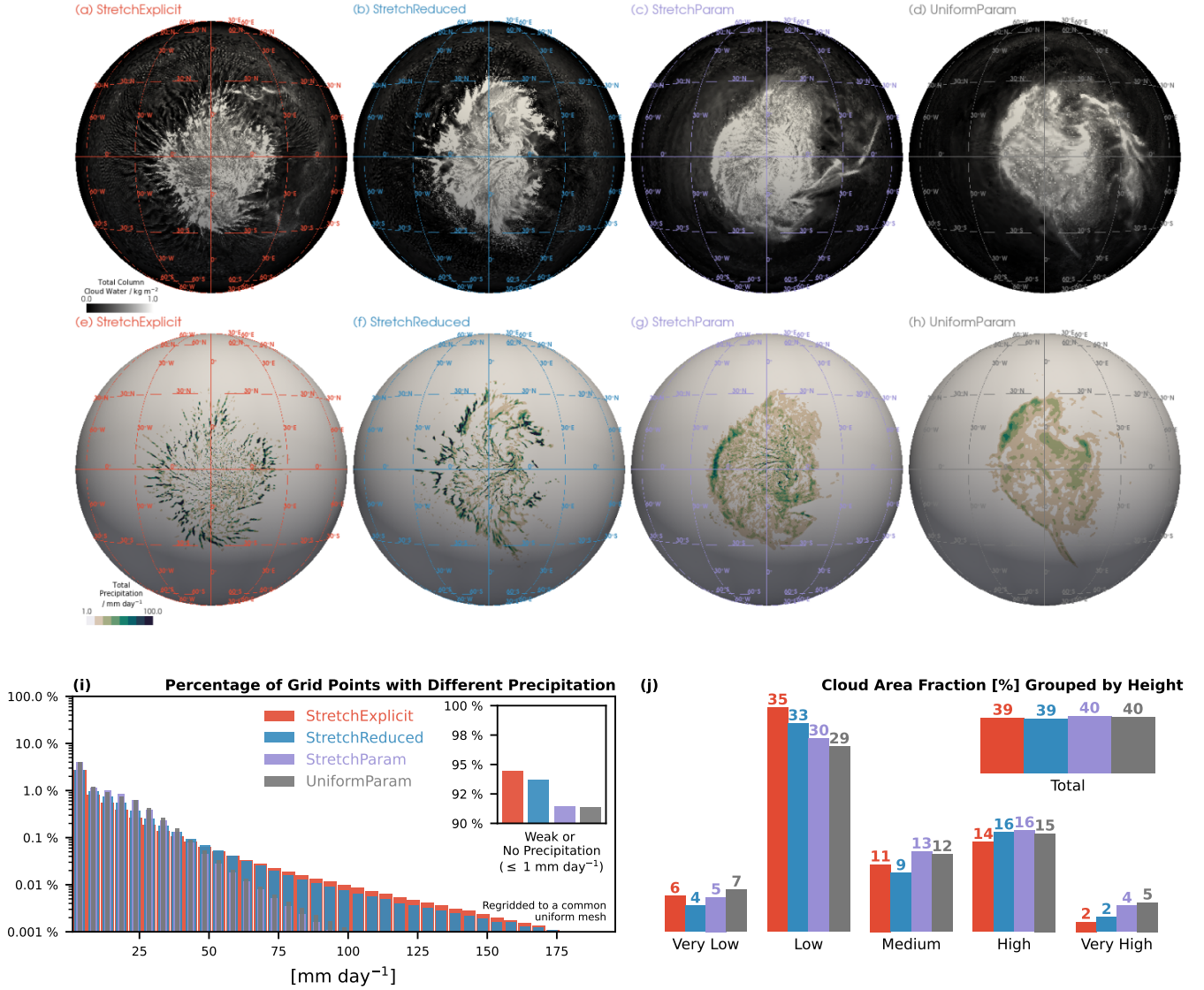


Figure 2. Clouds and precipitation in the simulations with stretched (*StretchExplicit*, *StretchReduced*, *StretchParam*) and quasi-uniform (*UniformParam*) mesh. (a–d) Maps of instantaneous vertically integrated cloud water (liquid plus ice) at the end of the simulations (kg m²). (e–h) Maps of instantaneous precipitation rate (mm day⁻¹). The substellar point is at the center of the maps (0°N, 0°E). (i) Histogram of instantaneous precipitation rate interpolated to a common quasi-uniform mesh as in the *UniformParam* simulation). The histogram shows the percentage of grid cells with precipitation above 1 mm day⁻¹, binned with a step of 5 mm day⁻¹. Note the logarithmic scale of the vertical axis. The inset shows the percentage of grid cells with precipitation below 1 mm day⁻¹ (weak or non-precipitating points). (j) Bar chart of cloud area fraction (%) grouped by different heights. Experimental setup is detailed in Fig 1 and Sec. 2.

reaches 100 mm day⁻¹ in the *UniformParam* simulation. Moving from a quasi-uniform to a stretched mesh has little effect (Fig. 2g), while reducing or disabling the convection scheme results in almost doubling of the maximum precipitation rate (Fig. 2e,f). The histogram in Fig. 2i distills this change in the precipitation maxima. It shows that the mesh stretching barely changes precipitation rates (after interpolating the data to the same mesh). However, reducing the impact of the convection scheme or even entirely switching it off results in substantially more intense precipitation, reaching 175 mm day⁻¹ at least twice within our analysis period of 500 days (0.001% of 221184 mesh cells). This is because in the *StretchExplicit* and *StretchReduced* cases much of the convection is handled by the grid-scale dynamics, permitting the formation of small but concentrated storms. Similarly high precipitation rate was reported

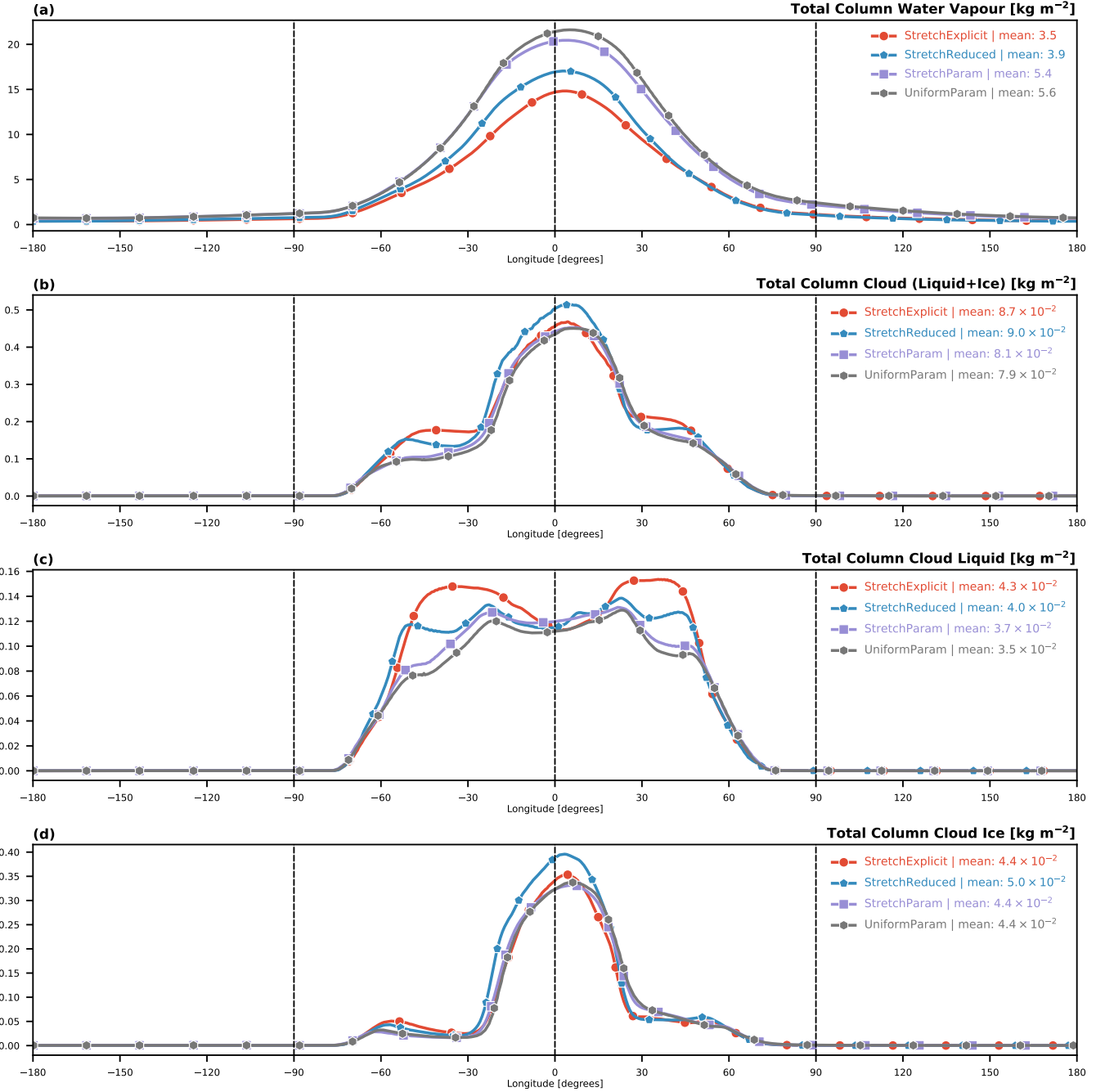


Figure 3. Meridional and time mean profiles of vertically integrated moisture diagnostics in kg m^{-2} : (a) water vapor, (b) total cloud (liquid plus ice), (c) cloud liquid, (d) cloud ice.

for the stretched-mesh simulations of Earth as an aquaplanet [Harris et al. \(2016\)](#) and for the convection-permitting limited-area simulations of the climate of TRAPPIST-1e and Proxima Centauri b ([Sergeev et al. 2020](#)).

The main effects of explicit convection on the global climate are a reduction in atmospheric water vapor content and an increase in condensed cloud water. While the *UniformParam* and *StretchParam* cases have a similar amount of water vapor ($5.4\text{--}5.6 \text{ kg m}^{-2}$), in the *StretchReduced* and *StretchExplicit* cases it decreases by about 25%, with the latter simulation being the driest overall (Fig. 3a). The overall drying of the atmosphere in the *StretchExplicit* and *StretchReduced* simulations is evident in the vertical profiles of absolute humidity (Fig. 3b) and relative humidity (Fig. 3c). The relative humidity is noticeably lower in the troposphere in the *StretchExplicit* and *StretchReduced*

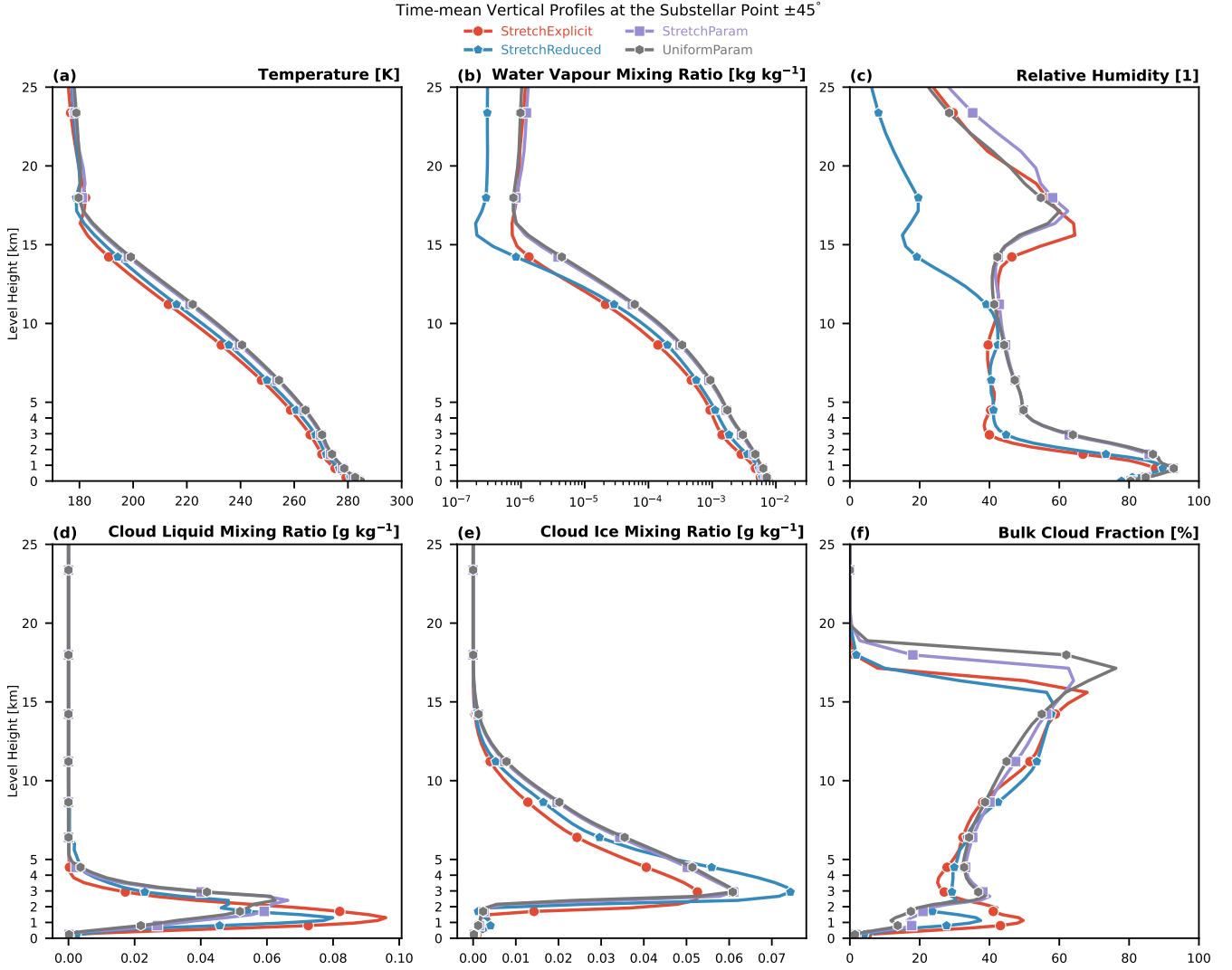


Figure 4. Vertical profiles of time mean diagnostics in the substellar region within the bottom 25 km of the atmosphere: (a) temperature in K, (b) water vapor mixing ratio in kg kg^{-1} , (c) relative humidity in %, (d) cloud liquid mixing ratio in g kg^{-1} , (e) cloud ice mixing ratio in g kg^{-1} , (f) cloud fraction in %.

simulations, so the water vapor decrease cannot be explained only by the lower temperatures in these two simulations (Fig. 3a). Indeed, since the stratospheric temperature is broadly the same in all four cases, it is the configuration of the convection scheme in the *StretchReduced* case that yields a less efficient upward transport of water vapor. This leads to a lower humidity in the upper layers of the night side and terminator regions (not shown), which may have a small effect on the water features in the transmission spectrum as discussed e.g. in Fauchez et al. (2022) and Sergeev et al. (2022a).

At the same time, the global amount of cloud water increases from 7.9×10^{-2} in the *UniformParam* experiment to 9×10^{-2} and $8.7 \times 10^{-2} \text{ kg m}^{-2}$ in the *StretchReduced* and *StretchExplicit* experiments, respectively (Fig. 3b). The largest increase of cloud condensate for the *StretchExplicit* case is seen in the liquid phase (Fig. 3c). It happens predominantly in the ring around the substellar region, i.e. where the grid resolution becomes relatively coarse due to the nature of the mesh stretching. The grid spacing is too large to fully resolve the shallow convection, and the representation of convective updrafts suffers from the lack of parameterization that can remove the instability. Explicit convection overcompensates for this, and as a result, convective updrafts remove moisture out of the boundary layer too efficiently, creating more cloud condensate (evident especially in the liquid cloud content in Fig. 3c). In the *StretchReduced* experiment, the parameterizations are set up to represent shallow convection better. As a result, grid-aliased convection

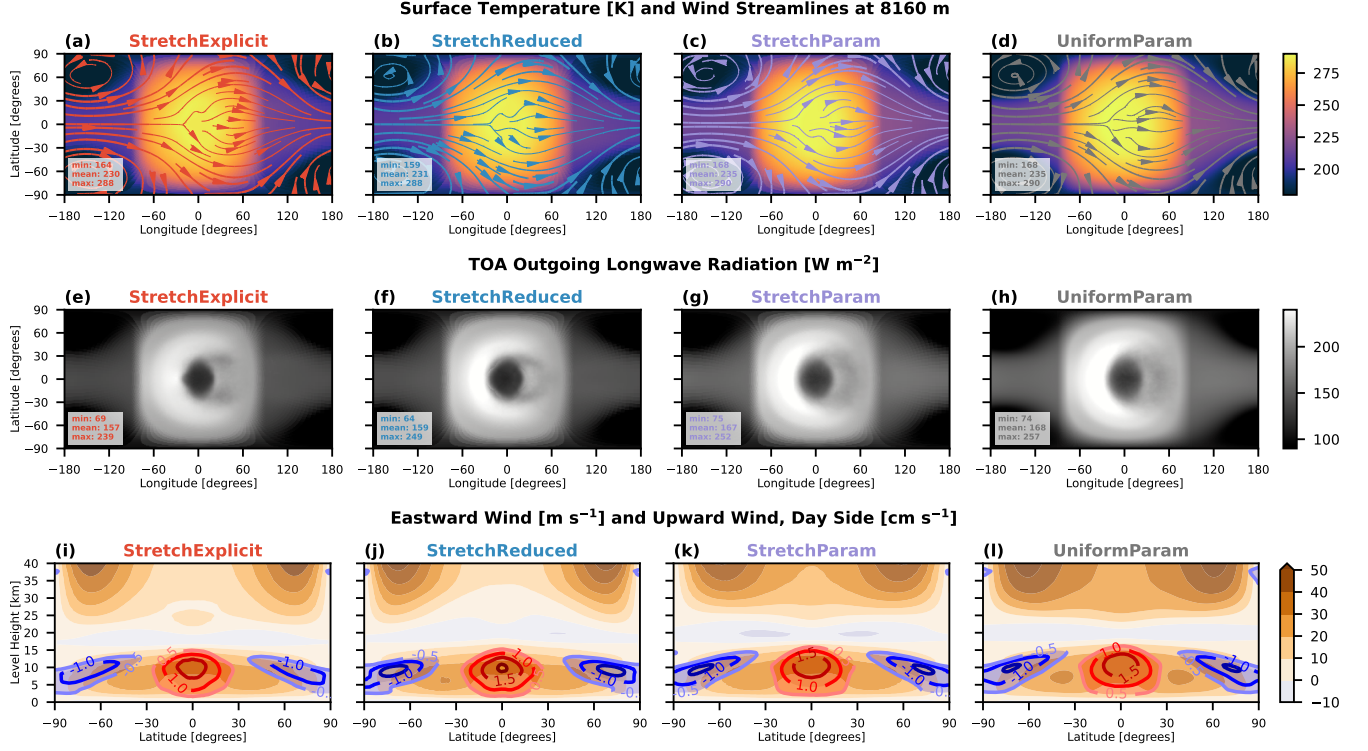


Figure 5. Time mean thermodynamic and circulation regime in our simulations. (a–d) Surface temperature in K overlaid by streamlines of the horizontal wind at ≈ 8 km above the surface. (e–h) Top-of-atmosphere outgoing longwave radiation in W m^{-2} . (i–l) Zonal mean of the eastward wind (orange contours, m s^{-1}) overlaid by the day-side upward wind (red and blue contours, cm s^{-1}).

is not as intense, and the cloud content around the substellar region is lower than that in the *StretchExplicit* case (Fig. 3c,d). The liquid cloud increase in the reduced and explicit convection simulations contributes to the changes in the cloud fraction. As Fig. 2j reveals, moving from parameterized convection (*StretchParam* and *UniformParam*) to reduced/explicit convection (*StretchReduced* and *StretchExplicit*), the global-mean low cloud fraction increases by up to 6%. This change happens predominantly in the substellar region, and is indeed due to the liquid phase increase, as evident in the vertical profiles of the mixing ratio and bulk cloud fraction (Fig. 4d,f).

The cloud cover differences between the parameterized and explicit convection experiments lead to changes in the radiation balance and, consequently, the surface temperature. In the *StretchExplicit* case, the top-of-atmosphere short-wave cloud radiative effect is -58.8 W m^{-2} , more than 10 W m^{-2} greater in magnitude than that in the *UniformParam* case. A similar brightening of clouds was reported in Tomassini et al. (2023) for the reduced convection experiments. Expressed in terms of the global mean albedo, the amount of reflected shortwave radiation ranges from 21.9% in the *UniformParam* case to 25.2% in the *StretchExplicit* case. Together with the reduction in the greenhouse effect due to less water vapor, this leads to a 5 K drop in the global mean surface temperature in the *StretchExplicit* case (Fig. 5a–d). The global mean surface temperature is 230, 231, 235 and 235 K in the *StretchExplicit*, *StretchReduced*, *StretchParam*, and *UniformParam*, respectively. Note that the *StretchReduced* climate is not colder than *StretchExplicit* despite having a substantially lower stratospheric humidity (Fig. 3b). This is because the greenhouse effect of the stratospheric water vapor is small due to its very low absolute amount.

The thermal maps in our simulations exhibits a day-night dichotomy typical for tidally locked planets, both in terms of surface temperature (Fig. 5a–d) and top-of-atmosphere outgoing longwave radiation (Fig. 5e–h). The substellar area reaches temperatures of 288–290 K, while the night-side coldest areas (stationary gyres) reach temperatures of 159–168 K. The latter substantially lower than the value predicted by a coarse-mesh LFRic-Atmosphere simulations of the THAI Hab 1 case (Sergeev et al. 2023), which is likely due to the slower rotation rate of the planet in the present study. Likewise, the outgoing longwave radiation is at the lower end of the THAI inter-model spread (Sergeev et al. 2022b): its values range from 167.8 W m^{-2} in the *UniformParam* experiment to 156.8 W m^{-2} in *StretchExplicit*

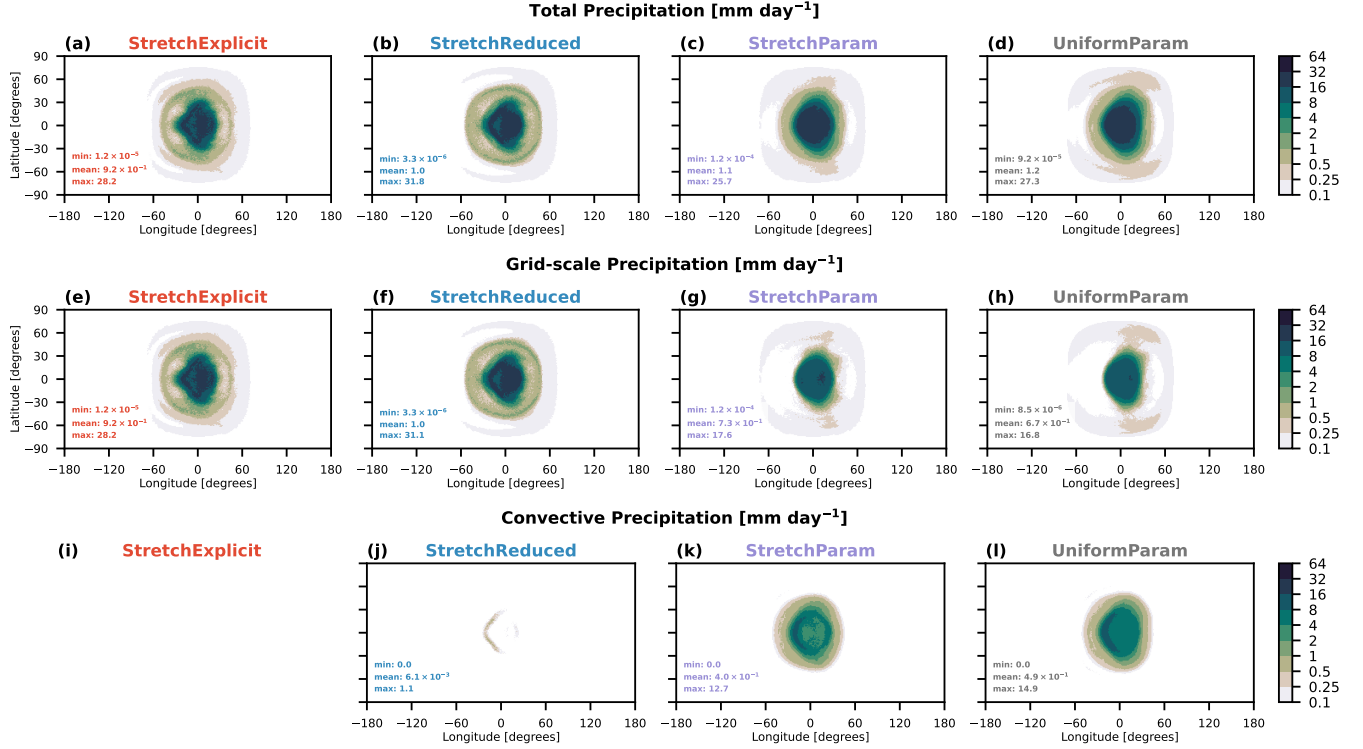


Figure 6. Maps of time mean precipitation rate in mm day^{-1} , from top to bottom: total, grid-scale, convective. Note that there is no convective precipitation in the *StretchExplicit* simulation, because the convection parameterization is switched off.

(Fig. 5e–h). Clouds prevent even more heat being lost to space, so their net effect on the top-of-atmosphere longwave radiation flux is positive. It is broadly the same in our four experiments ($\approx 13 \text{ W m}^{-2}$) and is comparable to that predicted by the models in [Sergeev et al. \(2022b\)](#) and [Yang et al. \(2023\)](#).

In agreement with the global temperature distribution, the large-scale circulation is broadly the same in all four simulations (see streamlines in Fig. 5a–d). The main pattern of the wind field in the troposphere is a superrotating (prograde) jet at the equator and stationary cyclonic gyres in high latitudes on the night side, as is typically expected for synchronously rotating terrestrial planets (e.g. [Haqq-Misra et al. 2018](#); [Komacek & Abbot 2019](#); [Hammond et al. 2020](#)). The vertical structure of the wind field reveals that the atmosphere has two regions of eastward flow: tropospheric (below $\approx 15 \text{ km}$) and stratospheric (above $\approx 25 \text{ km}$), with a quiescent region in between (Fig. 5i–l). The tropospheric flow is characterized by intense upward motions in the substellar region (red contours in Fig. 5i–l), associated with convergence near the surface and divergence aloft. The zonal-mean vertical velocity is marginally stronger in the *StretchReduced* simulation, which is due to the changes in the convection parameterization. Mesh stretching alone brings a relatively small change in the time-averaged vertical velocity (Fig. 5k). In the stratosphere, the eastward flow has two maxima in high latitudes, which become somewhat weaker moving from *UniformParam* to *StretchExplicit*. Hence, the 3D wind field in our simulations is broadly similar to and only slightly weaker than that in the Unified Model output for THAI Hab 1 ([Sergeev et al. 2022b](#)).

Despite better resolving small-scale convective patterns (Fig. 2), on average our stretched-mesh simulations produce a similar total precipitation rate as compared to that in the non-stretched-mesh simulations with parameterized convection (Fig. 6). The precipitation rate has a broad peak over the substellar region, reaching $\approx 30 \text{ mm day}^{-1}$ at the substellar point — close to the highest values within the inter-tropical convergence zone in [Harris et al. \(2016\)](#). Averaged meridionally (across all latitudes), the peak of precipitation is about 10 mm day^{-1} (not shown) and agrees well with the values in [Yang et al. \(2023\)](#). However, the way the model generates precipitation is different. Grid-scale precipitation, generated by the microphysics scheme, is the largest in the *StretchExplicit* and *StretchReduced* cases, accounting for almost all of the precipitation in these cases (Fig. 6e,f). Convective precipitation, on the other hand, the largest in the *UniformParam* case, and second-largest in *StretchParam*: $\approx 0.4 \text{ mm day}^{-1}$ (Fig. 6k,l). In the

StretchReduced simulation, the reduced convection parameterization yields about two orders of magnitude less precipitation than the full parameterization. This is because the *StretchReduced* simulation has a larger convective available potential energy (CAPE) time scale (Appendix B), which is a key parameter controlling the amount of parameterized convective mass flux relative to the resolved vertical motion and associated rainfall in the model (Tomassini et al. 2023). In summary, stretching the mesh while keeping the convection parameterization the same results in relatively more grid-scale precipitation; while reducing or disabling this parameterization offloads the precipitation to the grid scale.

4. DISCUSSION

Our results show that LFRic-Atmosphere is capable of simulating small-scale atmospheric processes using a stretched mesh while also reproducing the key characteristics of the global climate of a tidally locked terrestrial exoplanet. Using a locally refined mesh allows us to capture small-scale cloud patterns in the substellar region. This includes the banded cloud structures on the day side of the planet, known as “cloud streets” previously examined in convection-permitting simulations in Yang et al. (2023). In agreement with previous studies based on localized or global high-resolution grids (e.g. Harris et al. 2016; Kajikawa et al. 2016; Uchida et al. 2016; Rios-Berrios et al. 2022), resolving deep convection leads to more intense and localized precipitation. Thus, at a reduced computational cost (Table 1), LFRic-Atmosphere allows us to examine a regional phenomenon such as convection in great detail and at the same time study the interaction between local and global atmospheric circulation. Tidally locked exoplanets offer a particularly suitable use case but a locally refined mesh has also shown potential for Mars climate modeling, e.g. at the scale of individual craters (Lian & Richardson 2023).

Our study is the first exoplanet application of LFRic-Atmosphere in a global configuration with explicit convection, allowed for by the stretched mesh. Our key finding is that the simulation with explicit convection (*StretchExplicit*) predicts a climate that is substantially drier (as seen in both specific and relative humidity) and colder (by ≈ 5 K), with about 10% more cloud condensate compared to the simulations with fully parameterized convection. The main reason for the colder climate is the higher cloud albedo, i.e. stronger reflection of the shortwave radiation by clouds (by ≈ 10 W m⁻²). Additionally, there is less water vapor and thus a weaker greenhouse effect. The increase in cloud condensate, especially in the low-level cloud liquid, can be partly explained by the fact that the grid resolution on the day side’s periphery may be too coarse to fully resolve the shallow convection. However, the experiment with reduced parameterization (*StretchReduced*) produces a similar cloud structure (between that in the *StretchExplicit* run and those with fully parameterized convection), supporting this trend. We believe that overall our experiment with explicit convection produces a simulated climate closer to reality because it truly represents the underlying physics of the atmosphere, without relying on parameterizations tuned for Earth. In the absence of observational constraints, these simulations may serve as benchmarks for coarse-resolution GCMs with parameterized convection. At the same time, as noted in Tomassini et al. (2023), cloud parameterizations will likely require tuning for convection-permitting models. This may reduce the amount of shortwave radiation reflected by the clouds, resulting in a warmer climate. Future work should explore the representation of cloud microphysics and their impact on the climate in stretched-mesh simulations.

A caveat of the present study is that the convection scheme in our model is not tuned for a stretched mesh configuration. Indeed, in most km-scale models convection is only partially resolved (Tomassini et al. 2023). This introduces the challenge of representing convection in a balanced way: partially explicitly and partially as a parameterized sub-grid process. Scale-aware convection schemes are a promising solution (Kendon et al. 2021), which may also re-ignite interest in using stretched-mesh GCMs (Uchida et al. 2016). One example of a scale-aware scheme is CoMorph, a new convection parametrization under development at the Met Office (Daleu et al. 2023; Lavender et al. 2024). It is designed for use within both the Unified Model and LFRic-Atmosphere and has already shown to be close to cloud-resolving models in representing many aspects of convection (Lavender et al. 2024). The benefits of applying CoMorph in a stretched-mesh configuration will be explored for a tidally locked exoplanet in a future study.

Despite the differences discussed above, the key climate diagnostics and spatial patterns simulated in the stretched and non-stretched runs are relatively similar and the fidelity of the large-scale atmospheric circulation is preserved. We have thus shown that mesh stretching allows for a gradual transition into high resolution and does not produce numerical artifacts, confirming previous work on Earth climate (Fox-Rabinovitz et al. 2000; Harris et al. 2016; Uchida et al. 2016) and opening new avenues for studying 3D mixing in planetary atmospheres.

We thank Lorenzo Tomassini for his help with the reduced convection setup. We thank Thomas Melvin and Nigel Wood for helpful feedback on this work. We thank Thomas Melvin for his help with the cubed sphere mesh visualization. Material produced using Met Office Software. We acknowledge use of the Monsoon2 system, a collaborative facility supplied under the Joint Weather and Climate Research Programme, a strategic partnership between the Met Office and the Natural Environment Research Council. Additionally, some of this work was performed using the DiRAC Data Intensive service at Leicester, operated by the University of Leicester IT Services, which forms part of the STFC DiRAC HPC Facility (www.dirac.ac.uk). The equipment was funded by BEIS capital funding via STFC capital grants ST/K000373/1 and ST/R002363/1 and STFC DiRAC Operations grant ST/R001014/1. DiRAC is part of the National e-Infrastructure. This work was supported by a UKRI Future Leaders Fellowship MR/T040866/1. This work also was partly funded by the Leverhulme Trust through a research project grant RPG-2020-82.

Software: The LFRic-Atmosphere source code and configuration files are freely available from the Met Office Science Repository Service (<https://code.metoffice.gov.uk>) upon registration and completion of a software license. The UM and JULES code used in the publication has been committed to the UM and JULES code trunks, having passed both science and code reviews according to the UM and JULES working practices; in the UM/JULES versions stated in the paper (vn13.3). Scripts to post-process and visualize model output are available at https://github.com/dennissergeev/stretched_mesh_code and depend on the following open-source Python libraries: `aeolus` (Sergeev & Zamyatina 2022), `geovista` (Little 2023), `iris-esmf-regrid` (Worsley 2023), `iris` (Met Office 2023), `matplotlib` (Hunter 2007), and `numpy` (Harris et al. 2020).

APPENDIX

A. MESH STRETCHING

The stretching of the mesh is achieved using the Schmidt (1977) transformation (see also Harris et al. 2016; Bindle et al. 2021). It preserves the mesh topology, so the number of grid points and their connectivity are the same as in the non-stretched mesh (Fig. 1d). The stretching is smooth and does not have abrupt transitions in resolution such as those associated with grid nesting (Sergeev et al. 2020). The resulting grid has a refined resolution at the target location compensated by a coarser resolution on the opposite side of the sphere. Finally, the refined domain (the ‘target face’) diminishes in size proportional to the stretching factor.

The mesh stretching procedure involves two steps. First, the grid points of the original cubed sphere are attracted to the South Pole by the Schmidt (1977) transform

$$\phi'(\phi) = \arcsin\left(\frac{D + \sin \phi}{1 + D \sin \phi}\right) \quad \text{with } D = \frac{1 - S^2}{1 + S^2},$$

where S is the stretch factor ($S > 1$ causes stretching), ϕ is the original latitude, and ϕ' is the transformed latitude. The second step is the rotation of the stretched mesh so that the refined region is centered at the desired location. Thus, four parameters uniquely define a stretched mesh: the size of the cubed sphere C_n , the stretch factor S , the target latitude ϕ_T and longitude λ_T . The larger the S factor, the finer and more localized the refinement is. The grid spacing at the target location is approximately S times finer compared to the non-stretched mesh, while at the antipode location it is approximately S times coarser. Stretch factors used in existing literature are typically between 2.5 and 10 (e.g. Fox-Rabinovitz et al. 2006; Harris et al. 2016; Uchida et al. 2016; Bindle et al. 2021).

As shown in Fig. 1, we use a stretched mesh with $s = 10$ which gives a resolution $\approx 10\times$ finer at the target location. The target location is the substellar point $\phi_T = 0^\circ$, $\lambda_T = 0^\circ$. While the factor of 10 is high, it has been used for Earth applications, e.g. to better resolve nitrogen dioxide emissions in California (Bindle et al. 2021). By using a highly stretched mesh, we also test the boundaries of the computational stability of LFRic-Atmosphere. In future studies, we will probe other stretch factors, depending on the planet and problem in question.

The resulting stretched mesh has a cell width size of $\approx 4.7\text{km}$ in the substellar region (Fig. 1a–c), reaching the convection-permitting resolution. To achieve a similar resolution with a quasi-uniform mesh, one would have to use 100 times as many grid points, which is extremely computationally expensive for climate simulations. Similar 4-km grid spacing has been used for simulating convection explicitly in regional climate predictions for Earth (e.g. Stratton et al. 2018) and, more recently, for exoplanets with an Earth-like atmosphere, both on a global (Yang et al. 2023)

Table 1. Technical details of the experiments.

| | <i>StretchExplicit</i> | <i>StretchReduced</i> | <i>StretchParam</i> | <i>UniformParam</i> |
|--|---|-----------------------|---------------------|---------------------|
| Mesh | C192 | | | |
| Number of columns | 221184 | | | |
| Stretch factor S | 10 | 10 | 10 | 1 (no stretching) |
| Number of vertical levels | 63 | | | |
| Model top (km) | 41.02239 | | | |
| Dynamics time step (seconds) | 120 | 120 | 120 | 300 |
| Radiative transfer time step (seconds) | 1200 | | | |
| System configuration | Cray XC-40 Broadwell Nodes (36 CPUs per node) | | | |
| Number of cores | 864 | | | |
| Relative wall time per model time | 1.92 | 2.09 | 2.18 | 1.00 |
| Relative throughput (model time per wall time) | 0.52 | 0.48 | 0.46 | 1.00 |

and regional (Sergeev et al. 2020) scale. By the nature of grid stretching, the night side of the planet has a relatively coarse mesh spacing of up to ≈ 470 km. Nevertheless, even this resolution is close to those applied *globally* in previous studies for exoplanetary climates (e.g. Yang et al. 2013; Turbet et al. 2016; Paradise et al. 2022).

As Table 1 shows, the cost of performing stretched-mesh simulations is only about $2\times$ higher than that of the uniform-mesh simulation (mostly due to a smaller time step in the stretched-mesh setup), while allowing us to reach a convection-permitting resolution for the substellar point. Using a uniform mesh with the same high resolution for the whole planet would require a relative computational cost of ~ 1000 .

B. CONVECTION AND TURBULENCE PARAMETERS IN THE *StretchReduced* EXPERIMENT

In the *StretchReduced* experiment, we follow a km-scale configuration used for the Unified Model in Tomassini et al. (2023), namely their *MidLevShConv15RA turb* configuration. This configuration combines a reduced convection parameterization with a modified representation boundary layer scheme. As a result, convection is allowed to be partly explicit, accounting for the fact that in the focal region of our stretched mesh the grid step reaches 4.7 km.

Briefly, the *StretchReduced* parameterization settings are different to those used in *StretchParam* and *UniformParam* in the following. Scaling of the shallow convective mass flux is set to 0.015 (default: 0.03) — the value found to produce more realistic low-level clouds in global km-scale numerical weather prediction runs. The formulation of the mid-level convection scheme is also modified. The key modification that reduces the sub-grid convective mass flux according to the model resolution, allowing convection to be partly explicit, is a longer timescale for the convective available potential energy (CAPE) closure (2700 s instead of the default 1800 s). The configuration also includes the turbulence blending scheme (Boutle et al. 2014), which allows for a transition between the 1D turbulence parameterization (used in coarse-grid GCMs) with a 3D Smagorinsky-Lilly turbulence scheme (used in cloud-resolving models).

C. CIRCULATION REGIME BISTABILITY

In additional experiments, we change the rotation rate of TRAPPIST-1e to show the climate bistability. We set it to its observed orbital period of 6.1 days, i.e. the value prescribed by the THAI protocol (Faucher et al. 2020) and used in the majority of modeling studies for this planet (e.g. Wolf 2017; Turbet et al. 2018; Faucher et al. 2019; Eager-Nash et al. 2020; May et al. 2021; Turbet et al. 2022; Yang et al. 2023). Broadly, our conclusions hold for these simulations. The key difference is that in this case the GCM is prone to a climate bistability: the atmospheric circulation settles on a double-jet regime in the *StretchExplicit* experiment, and on a single-jet regime in the other three experiments (for definitions, see Sergeev et al. 2022a). This corresponds to a distinct difference in climate characteristics, including the

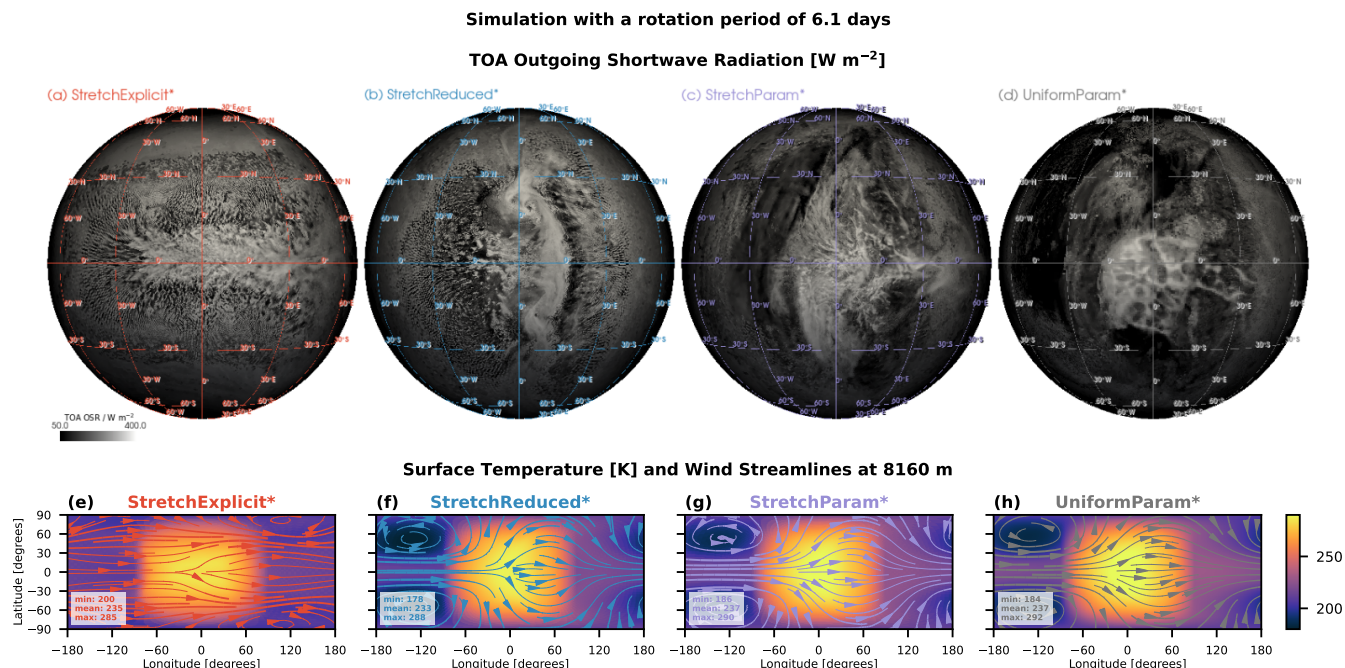


Figure 7. Circulation regime bistability in the simulations with the rotation period set to 6.1 days. The circulation regime switches to another state when the convection scheme is switched off — compare the two leftmost columns (the *StretchExplicit* and *StretchReduced* cases). Top panels show instantaneous top-of-atmosphere outgoing shortwave radiation. Bottom panels show the time mean surface temperature in K overlaid by streamlines of the horizontal wind at ≈ 8 km above the surface.

global cloud cover (Fig. 7). In the *StretchExplicit* experiment, the cloud cover associated with the deep convection is narrower and more zonally elongated than that in the other three experiments.

The fact that the circulation regime changes not when the mesh is stretched (comparing *UniformParam* to *StretchParam*) but when the convection scheme is disabled (comparing *StretchParam* to *StretchExplicit*), confirms our key finding that for the global climate mesh stretching is less important than changes in model parameterizations (see Sec. 3). Furthermore, our *StretchExplicit* experiment is qualitatively similar to the convection-permitting simulation of TRAPPIST-1e in Yang et al. (2023), in terms of the spatial distribution of temperature, wind, cloud cover, and precipitation. This implies that at least some of the differences between the coarse-grid GCMs and the convection-permitting model reported by Yang et al. are due to the circulation regime change and not due to resolving convection per se. And as Sergeev et al. (2022a) demonstrated, the circulation regime change can happen even in a coarse-grid GCM if the convection parameterization is switched off or modified.

REFERENCES

- Adams, S., Ford, R., Hambley, M., et al. 2019, Journal of Parallel and Distributed Computing, 132, 383, doi: [10.1016/j.jpdc.2019.02.007](https://doi.org/10.1016/j.jpdc.2019.02.007)
- Arakawa, A. 2004, Journal of Climate, 17, 2493, doi: [10.1175/1520-0442\(2004\)017<2493:RATCPP>2.0.CO;2](https://doi.org/10.1175/1520-0442(2004)017<2493:RATCPP>2.0.CO;2)
- Bendall, T. M., Gibson, T. H., Shipton, J., Cotter, C. J., & Shipway, B. 2020, Quarterly Journal of the Royal Meteorological Society, 146, 3187, doi: [10.1002/qj.3841](https://doi.org/10.1002/qj.3841)
- Bendall, T. M., Wood, N., Thuburn, J., & Cotter, C. J. 2022, Quarterly Journal of the Royal Meteorological Society, doi: [10.1002/qj.4406](https://doi.org/10.1002/qj.4406)
- Bindle, L., Martin, R. V., Cooper, M. J., et al. 2021, Geoscientific Model Development, 14, 5977, doi: [10.5194/gmd-14-5977-2021](https://doi.org/10.5194/gmd-14-5977-2021)
- Boutle, I. A., Eyre, J. E. J., & Lock, A. P. 2014, Monthly Weather Review, 142, 1655, doi: [10.1175/MWR-D-13-00229.1](https://doi.org/10.1175/MWR-D-13-00229.1)
- Brown, A., Bendall, T. M., Boutle, I., Melvin, T., & Shipway, B. 2023, Physics-Dynamics-Chemistry Coupling Across Different Meshes in LFRic-Atmosphere: Formulation and Idealised Tests, arXiv, doi: [10.48550/arXiv.2310.01255](https://doi.org/10.48550/arXiv.2310.01255)

- Daleu, C. L., Plant, R. S., Stirling, A. J., & Whittall, M. 2023, *Quarterly Journal of the Royal Meteorological Society*, n/a, doi: [10.1002/qj.4547](https://doi.org/10.1002/qj.4547)
- Eager-Nash, J. K., Reichelt, D. J., Mayne, N. J., et al. 2020, *Astronomy & Astrophysics*, 639, A99, doi: [10.1051/0004-6361/202038089](https://doi.org/10.1051/0004-6361/202038089)
- Fauchez, T. J., Turbet, M., Villanueva, G. L., et al. 2019, *The Astrophysical Journal*, 887, 194, doi: [10.3847/1538-4357/ab5862](https://doi.org/10.3847/1538-4357/ab5862)
- Fauchez, T. J., Turbet, M., Wolf, E. T., et al. 2020, *Geosci. Model Dev*, 13, 707, doi: [10.5194/gmd-13-707-2020](https://doi.org/10.5194/gmd-13-707-2020)
- Fauchez, T. J., Villanueva, G. L., Sergeev, D. E., et al. 2022, *The Planetary Science Journal*, 3, 213, doi: [10.3847/PSJ/ac6cfl](https://doi.org/10.3847/PSJ/ac6cfl)
- Fox-Rabinovitz, M., Cote, J., Dugas, B., et al. 2008, *Meteorology and Atmospheric Physics*, 100, 159, doi: [10.1007/s00703-008-0301-z](https://doi.org/10.1007/s00703-008-0301-z)
- Fox-Rabinovitz, M., Côté, J., Dugas, B., Déqué, M., & McGregor, J. L. 2006, *Journal of Geophysical Research: Atmospheres*, 111, doi: [10.1029/2005JD006520](https://doi.org/10.1029/2005JD006520)
- Fox-Rabinovitz, M. S. 2000, *Journal of Geophysical Research: Atmospheres*, 105, 29635, doi: [10.1029/2000JD900650](https://doi.org/10.1029/2000JD900650)
- Fox-Rabinovitz, M. S., Stenchikov, G. L., Suarez, M. J., Takacs, L. L., & Govindaraju, R. C. 2000, *Monthly Weather Review*, 128, 1883, doi: [10.1175/1520-0493\(2000\)128<1883:AUAVRS>2.0.CO;2](https://doi.org/10.1175/1520-0493(2000)128<1883:AUAVRS>2.0.CO;2)
- Gryschka, M., & Raasch, S. 2005, *Geophysical Research Letters*, 32, 1, doi: [10.1029/2005GL022872](https://doi.org/10.1029/2005GL022872)
- Hammond, M., Tsai, S.-M., & Pierrehumbert, R. T. 2020, *The Astrophysical Journal*, 901, 78, doi: [10.3847/1538-4357/abb08b](https://doi.org/10.3847/1538-4357/abb08b)
- Haqq-Misra, J., Wolf, E. T., Joshi, M., Zhang, X., & Koppurapu, R. K. 2018, *The Astrophysical Journal*, 852, 67, doi: [10.3847/1538-4357/aa9flf](https://doi.org/10.3847/1538-4357/aa9flf)
- Harris, C. R., Millman, K. J., van der Walt, S. J., et al. 2020, *Nature*, 585, 357, doi: [10.1038/s41586-020-2649-2](https://doi.org/10.1038/s41586-020-2649-2)
- Harris, L. M., Lin, S.-J., & Tu, C. 2016, *Journal of Climate*, 29, 4293, doi: [10.1175/JCLI-D-15-0389.1](https://doi.org/10.1175/JCLI-D-15-0389.1)
- Hunter, J. D. 2007, *Computing in Science & Engineering*, 9, 90, doi: [10.1109/MCSE.2007.55](https://doi.org/10.1109/MCSE.2007.55)
- Jenney, A. M., Ferretti, S. L., & Pritchard, M. S. 2023, *Journal of Advances in Modeling Earth Systems*, 15, e2022MS003444, doi: [10.1029/2022MS003444](https://doi.org/10.1029/2022MS003444)
- Kajikawa, Y., Miyamoto, Y., Yoshida, R., et al. 2016, *Progress in Earth and Planetary Science*, 3, 16, doi: [10.1186/s40645-016-0094-5](https://doi.org/10.1186/s40645-016-0094-5)
- Kendon, E. J., Prein, A. F., Senior, C. A., & Stirling, A. 2021, *Philosophical Transactions of the Royal Society A: Mathematical, Physical and Engineering Sciences*, 379, 20190547, doi: [10.1098/rsta.2019.0547](https://doi.org/10.1098/rsta.2019.0547)
- Kent, J., Melvin, T., & Wimmer, G. A. 2023, *Geoscientific Model Development*, 16, 1265, doi: [10.5194/gmd-16-1265-2023](https://doi.org/10.5194/gmd-16-1265-2023)
- Komacek, T. D., & Abbot, D. S. 2019, *The Astrophysical Journal*, 871, 245, doi: [10.3847/1538-4357/aafb33](https://doi.org/10.3847/1538-4357/aafb33)
- Lavender, S. L., Stirling, A. J., Whittall, M., et al. 2024, *Quarterly Journal of the Royal Meteorological Society*, n/a, doi: [10.1002/qj.4660](https://doi.org/10.1002/qj.4660)
- Lefevre, M., Turbet, M., & Pierrehumbert, R. 2021, *The Astrophysical Journal*, 913, 101, doi: [10.3847/1538-4357/abf2c1](https://doi.org/10.3847/1538-4357/abf2c1)
- Lian, Y., & Richardson, M. I. 2023, *Planetary and Space Science*, 229, 105663, doi: [10.1016/j.pss.2023.105663](https://doi.org/10.1016/j.pss.2023.105663)
- Little, B. 2023, *geovista*, doi: [10.5281/zenodo.7608302](https://doi.org/10.5281/zenodo.7608302)
- May, E. M., Taylor, J., Komacek, T. D., Line, M. R., & Parmentier, V. 2021, *The Astrophysical Journal Letters*, 911, L30, doi: [10.3847/2041-8213/abeff](https://doi.org/10.3847/2041-8213/abeff)
- Melvin, T., Benacchio, T., Shipway, B., et al. 2019, *Quarterly Journal of the Royal Meteorological Society*, 145, 2835, doi: [10.1002/QJ.3501](https://doi.org/10.1002/QJ.3501)
- Melvin, T., Shipway, B., Wood, N., et al. 2024, A mixed finite-element, finite-volume, semi-implicit discretisation for atmospheric dynamics: Spherical geometry, arXiv, doi: [10.48550/arXiv.2402.13738](https://doi.org/10.48550/arXiv.2402.13738)
- Met Office. 2023, *Iris: A powerful, format-agnostic, and community-driven Python package for analysing and visualising Earth science data*, doi: [10.5281/zenodo.7948293](https://doi.org/10.5281/zenodo.7948293)
- Paradise, A., Macdonald, E., Menou, K., Lee, C., & Fan, B. L. 2022, *Monthly Notices of the Royal Astronomical Society*, 511, 3272, doi: [10.1093/mnras/stac172](https://doi.org/10.1093/mnras/stac172)
- Rios-Berrios, R., Bryan, G. H., Medeiros, B., Judt, F., & Wang, W. 2022, *Journal of Advances in Modeling Earth Systems*, 14, e2021MS002902, doi: [10.1029/2021MS002902](https://doi.org/10.1029/2021MS002902)
- Schmidt, F. 1977, *Contributions to Atmospheric Physics*, 50, 211, doi: [10.1186/s40645-014-0018-1.Schmidt](https://doi.org/10.1186/s40645-014-0018-1.Schmidt)
- Sergeev, D. E., Lambert, F. H., Mayne, N. J., et al. 2020, *The Astrophysical Journal*, 894, 84, doi: [10.3847/1538-4357/ab8882](https://doi.org/10.3847/1538-4357/ab8882)
- Sergeev, D. E., Lewis, N. T., Lambert, F. H., et al. 2022a, *The Planetary Science Journal*, 3, 214, doi: [10.3847/PSJ/ac83be](https://doi.org/10.3847/PSJ/ac83be)
- Sergeev, D. E., & Zamyatina, M. 2022, *Aeolus - a Python library for the analysis and visualisation of climate model output.*, doi: [10.5281/ZENODO.6478085](https://doi.org/10.5281/ZENODO.6478085)

- Sergeev, D. E., Fauchez, T. J., Turbet, M., et al. 2022b, *The Planetary Science Journal*, 3, 212, doi: [10.3847/PSJ/ac6cf2](https://doi.org/10.3847/PSJ/ac6cf2)
- Sergeev, D. E., Mayne, N. J., Bendall, T., et al. 2023, *Geoscientific Model Development*, 16, 5601, doi: [10.5194/gmd-16-5601-2023](https://doi.org/10.5194/gmd-16-5601-2023)
- Stratton, R. A., Senior, C. A., Vosper, S. B., et al. 2018, *Journal of Climate*, 31, 3485, doi: [10.1175/JCLI-D-17-0503.1](https://doi.org/10.1175/JCLI-D-17-0503.1)
- Tomassini, L., Willett, M., Sellar, A., et al. 2023, *Journal of Advances in Modeling Earth Systems*, 15, e2022MS003418, doi: [10.1029/2022MS003418](https://doi.org/10.1029/2022MS003418)
- Turbet, M., Leconte, J., Selsis, F., et al. 2016, *Astronomy & Astrophysics*, 596, A112, doi: [10.1051/0004-6361/201629577](https://doi.org/10.1051/0004-6361/201629577)
- Turbet, M., Bolmont, E., Leconte, J., et al. 2018, *Astronomy & Astrophysics*, 612, A86, doi: [10.1051/0004-6361/201731620](https://doi.org/10.1051/0004-6361/201731620)
- Turbet, M., Fauchez, T. J., Sergeev, D. E., et al. 2022, *The Planetary Science Journal*, 3, 211, doi: [10.3847/PSJ/ac6cf0](https://doi.org/10.3847/PSJ/ac6cf0)
- Uchida, J., Mori, M., Nakamura, H., et al. 2016, *Monthly Weather Review*, 144, 1423, doi: [10.1175/MWR-D-15-0271.1](https://doi.org/10.1175/MWR-D-15-0271.1)
- Walters, D., Baran, A. J., Boutle, I., et al. 2019, *Geoscientific Model Development*, 12, 1909, doi: [10.5194/gmd-12-1909-2019](https://doi.org/10.5194/gmd-12-1909-2019)
- Wei, M., Zhang, Y., & Yang, J. 2020, *The Astrophysical Journal*, 898, 156, doi: [10.3847/1538-4357/ab9b83](https://doi.org/10.3847/1538-4357/ab9b83)
- Wolf, E. T. 2017, *The Astrophysical Journal*, 839, L1, doi: [10.3847/2041-8213/aa693a](https://doi.org/10.3847/2041-8213/aa693a)
- Wolf, E. T., Kopparapu, R., Haqq-Misra, J., & Fauchez, T. J. 2022, *The Planetary Science Journal*, 3, 7, doi: [10.3847/PSJ/AC3F3D](https://doi.org/10.3847/PSJ/AC3F3D)
- Wordsworth, R., & Kreidberg, L. 2022, *Annual Review of Astronomy and Astrophysics*, 60, 159, doi: [10.1146/annurev-astro-052920-125632](https://doi.org/10.1146/annurev-astro-052920-125632)
- Worsley, S. 2023, *iris-esmf-regrid*. <https://github.com/SciTools-incubator/iris-esmf-regrid>
- Yang, J., Cowan, N. B., & Abbot, D. S. 2013, *The Astrophysical Journal*, 771, L45, doi: [10.1088/2041-8205/771/2/L45](https://doi.org/10.1088/2041-8205/771/2/L45)
- Yang, J., Zhang, Y., Fu, Z., et al. 2023, *Nature Astronomy*, 1, doi: [10.1038/s41550-023-02015-8](https://doi.org/10.1038/s41550-023-02015-8)
- Zhang, X., Tian, F., Wang, Y., Dudhia, J., & Chen, M. 2017, *The Astrophysical Journal*, 837, L27, doi: [10.3847/2041-8213/aa62fc](https://doi.org/10.3847/2041-8213/aa62fc)